Random and Ordered Defects on Ion-Bombarded Si(100)-(2×1) Surfaces

H. Feil and H. J. W. Zandvliet
Philips Research Laboratories, P.O. Box 80.000, 5600 JA Eindhoven, The Netherlands

M.-H. Tsai, John D. Dow, and I. S. T. Tsong
Department of Physics and Astronomy, Arizona State University, Tempe, Arizona 85287-1504
(Received 29 April 1992)

Scanning tunneling microscopy (STM) images of Si(100)-(2×1) surfaces bombarded by low-dose 3-keV Ar^+ ions showed random defects which ordered into line defects perpendicular to the dimer rows upon annealing at elevated temperatures. Molecular-dynamics simulations were performed to explain the shapes and sizes of the observed random defects and also to examine the stability of ordered defects. Our simulations showed good agreement with STM observations.

PACS numbers: 61.80.Jh, 68.55.Ln, 79.20.Rf

The process of sputtering, which involves the removal of individual atoms and molecules from a surface by energetic ions, has been a subject of interest for many decades. With the advent of scanning tunneling microscopy (STM), one has the means of viewing the surface damage due to sputtering with atomic resolution. In a recent experiment in which we bombarded Si(100)-(2×1) surfaces with 3-keV Ar^+ ions at low doses, i.e., $\sim 10^{12}$ ions cm^{-2} or $\sim 10^{-3}$ monolayer (ML), at room temperature, we reported the observation of random defects which ordered into line defects upon annealing the bombarded surfaces to 750 °C for 2 min [1]. The low-dose experiment is illustrated in Fig. 1. The starting Si(100)-(2×1) surface was remarkably free of any metal contamination which could give rise to line defects perpendicular to the dimer rows [2]. Figure 1(a) shows an STM image of such a surface, with single missing dimers being the predominant defects. Figure 1(b) shows the surface after bombardment by 3-keV Ar^+ ions at normal incidence with a dose of 1.5×10^{12} ions cm^{-2}, equivalent to ~ 0.002 ML coverage. A higher concentration of random defects was observed, some of which contain multiple missing dimers. When a bombarded surface was annealed at 600 °C for 2 min, the random defects appeared to order into line defects perpendicular to the dimer rows, as shown in Fig. 1(c). Annealing at higher temperatures, 750 and 850 °C for 2 min, produced the same effect as shown in Fig. 1(d). When the bombarded surface was annealed at 950 °C for 2 min, or flashed to 1200 °C for a few seconds, the surface was completely restored to that shown in Fig. 1(a), without any trace of line defects, thus ruling out the possibility of metal contamination which invariably worsens with each annealing cycle. We did not observe any ordering of the random defects when we annealed the surface at 500 °C for 2 min. This implies that the threshold temperature for ordering lies between 500 and 600 °C. Over 100 STM images were taken in our experiment and consistent results were obtained.

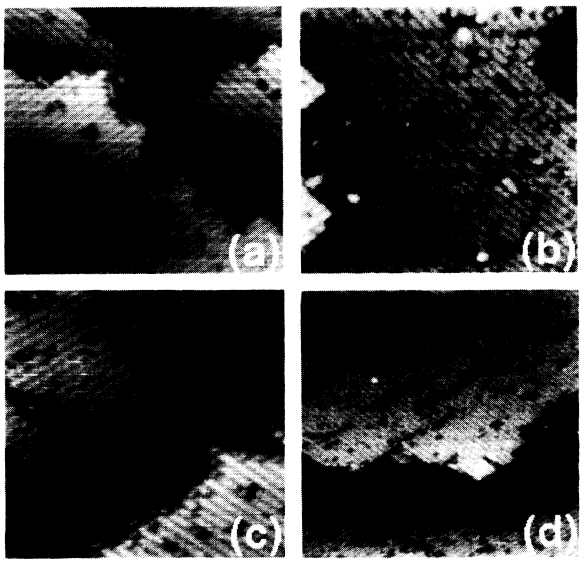

FIG. 1. Filled-state STM images of Si(100)-(2×1) surfaces taken at sample bias of −2 V and tunnel current 0.5 nA. (a) Clean surface prior to bombardment. Scan area is 28 nm×28 nm. (b) After bombardment by 3-keV Ar^+ ions at a dose of 1.5×10^{12} ions cm^{-2}. Scan area is 26 nm×26 nm. (c) Bombarded surface after annealing at 600 °C for 2 min. Scan area is 22 nm×22 nm. (d) Bombarded surface after annealing at 750 °C for 2 min. Scan area is 40 nm×40 nm.

The possibility exists that the line defects are not due to ordering of surface vacancies, but arise from the ordering of implanted Ar atoms diffusing to the surface during annealing. However, previous ellipsometry studies of desorption of implanted Ar from Si surfaces [3] show that desorption takes place at temperatures as low as 400 °C, reaching a maximum at 600 °C. Complete desorption is achieved at 800 °C and the Si surface returns to its original state [4]. These results do not agree with our observation that ordering occurs between 600 and 850 °C, and the line defects only disappear at 950 °C or upon flashing the surface to 1200 °C. Analysis of fourteen STM images taken before and after annealing shows that the number of vacancies increases on average by $\sim 15\%$ after annealing. A plausible cause for the increase is the migration of buried vacancies to the surface during the annealing process, or it could be the result of random sampling of the surface because the STM did not

© 1992 The American Physical Society

image the same localized area after annealing. The Gaussian distribution of the Ar^+ ions in the beam spot impacting the surface could also give rise to the counting discrepancy.

In this Letter, we compare our STM images with the results of molecular-dynamics (MD) simulations in order to understand the mechanisms which lead to the formation of the random and ordered defects on the surface bombarded by a low dose of Ar^+ ions.

In the classical MD simulations we have bombarded a dimerized Si(100) surface with individual 3-keV Ar^+ ions. The microcrystallite consists of 12 layers of 32 atoms each. Periodic boundary conditions are applied in order to minimize boundary effects. The bottom-layer atoms are coupled to their initial positions with a harmonic force. The value of the force constant is 10^{-8} $N m^{-1}$. A temperature control is added to mimic the heat flow to the bulk. The method described by Berendsen *et al.* [5] is used to couple all the atoms of the crystallite to an external bath at constant temperature. In the simulation, the coupling is to a bath at $T=300$ K with a time constant $\tau=400$ fs. With this value the crystallite is cooled down to 30 K within a few ps after the ion impact. In order to correct for the dissipation of energy due to the shock wave shortly after the impact, the potential energy buildup in the bottom atoms is removed from these atoms as long as their temperature exceeds the temperature of the external bath. In the case of events causing large surface damage, a larger crystallite is used containing 128 Si atoms in each layer. This size is large enough to prevent interference due to the periodic boundary conditions and the finite size of the crystallite. The Si-Si interactions are described by the Stillinger and Weber many-body potential [6]. To incorporate a more repulsive Si-Si interaction at short internuclear separations, the potential is splined between $r=1.09$ and 1.59 Å with a Moliere potential with a screening length of 0.83 times the Firsov value [7]. The attractive Ar-Ar and Si-Ar interactions are negligible under the experimental conditions. The nonbonding Ar-Si and Ar-Ar interactions are described by a Moliere potential, also with a screening length of 0.83 times the Firsov value. The individual trajectories are sensitive to the details of the short-range interactions such as small variations of the impact points of the incoming ion. Consequently, we performed statistical analysis on the simulations in much the same manner as we did on the experimental results.

A set of 30 trajectories is developed by random sampling of the representative area of the Si(100) surface. With every new trajectory, a fresh surface is bombarded with the ion. This approach simulates the low-dose experiment. In the simulated 30 events we have observed 21 sputtered atoms. The sputter yield compares well with the MD data of Smith, Harrison, and Garrison [8] and is somewhat lower than the experimental high-dose yield of ~ 1 atom/ion [9]. Only about one-third of the surface vacancies are created by sputter removal. The remaining vacancies are formed because Si atoms in the top layers are recoiled into the bulk. These recoil Si atoms are the beginning of collision cascades and in the 30 events, 57 Si atoms escaped through the bottom layer of the crystallite.

In six cases the simulation produced no surface damage. In the remaining simulations, we observed altogether 33 missing dimers, 25 defect dimers, 19 adatoms, and 11 adclusters. The damage is in the form of 17 small craters, 8 medium size craters, and 1 large crater. In a few cases, the ion impact created more than 1 crater, as shown in Fig. 2(a). A small crater corresponds to the area of about 1 dimer. A medium crater corresponds to a damaged area of about 2 dimers, while a large crater has an area of about 8 dimers. The classification is rather arbitrary and sometimes it is difficult to classify a crater in any one of the three categories. Examples of small, medium, and large craters are given in Figs. 2(b)–2(d).

Our simulations produced 26 craters from 30 ion impacts, i.e., ~ 1 crater per impact. From our STM images in Fig. 1, the clean surface in Fig. 1(a) shows ~ 60 defects, represented by dark spots in the image, while the bombarded surface in Fig. 1(b) shows ~ 125 defects or dark spots of various sizes. There is an increase of ~ 65 defects after bombardment. The ion dose in Fig. 1(b) was 1.5×10^{12} ions cm^{-2}, which translates into ~ 10 ion impacts on an area of the size shown in Fig. 1(b). So the number of additional defects is 6 times that of the ion impacts. From our STM images taken on Si(100)-(2×1) surfaces bombarded by doses varying from 7×10^{11} to 6×10^{12} ions cm^{-2}, we observed consistently more defects produced by the bombardment than the number of ion impacts. This sharply contrasts our observations on the Si(111)-(7×7) surface [1], on which we found the ratio

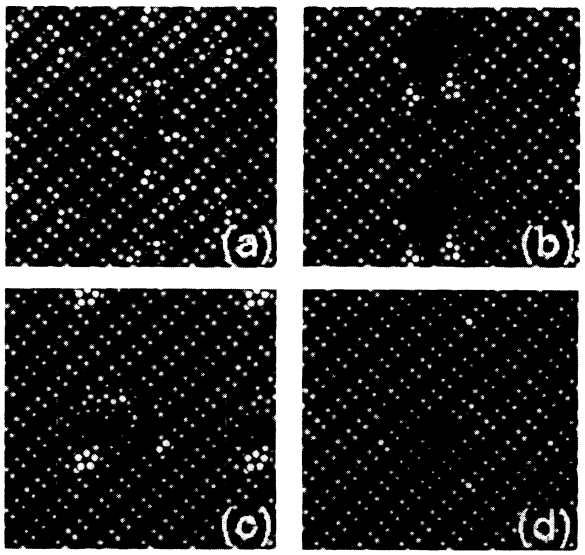

FIG. 2. Ion-impact craters produced by molecular-dynamics simulations. (a) A double crater. (b) A large crater. (c) A medium crater. (d) A small crater. The craters in (b) and (c) appear double because of periodic boundary conditions.

of defects (or craters) to ion impacts was ~1. The origin of this discrepancy could be that on Si(100), each ion impact creates more than 1 site from which sputtering occurs, as MD simulations show in Fig. 2(a). Some of the defects generated may also be electronic in origin rather than topographic, and they are unrelated to sputtering.

It is interesting to compare the large craters observed in the STM images with the large simulated crater shown in Fig. 2(b). Figure 3 shows two large experimental craters on the same scale as that in Fig. 2(b). There is a remarkable resemblance between experiment and simulation. In the simulated crater, we observe clusters of adatoms in the vicinity of the crater. We also observe large bright spots, which may be due to adclusters, near the large craters in the STM images.

Annealing at temperatures at or above 600 °C causes the random defects to order into narrow line defects as shown in Figs. 1(c) and 1(d). A possible origin of these line defects could be a preferential mobility of vacancies on the surface along the dimer rows [10] as a consequence of the annealing temperature, and the attractive interaction of the vacancies. The question of whether the line defects should be perpendicular or parallel to the dimer rows is examined by performing a microscopic study using a quantum-mechanical MD method. The advantage of using this method over the conventional total-energy calculational method is that atomic positions are automatically optimized according to Newton's laws of motion. In contrast, the conventional total-energy methods need to preconceive some preferred geometries. The MD method employed in this study is the *ab initio* real-space method of Sankey and Niklewski [11], which has been shown to work well for various systems of carbon and silicon [12–14].

In this study, the Si(100) surface is modeled by a five-layer-slab repeated slab (supercell) model; the atoms in the bottom layer are assigned with huge masses and attached with hydrogenlike atoms to saturate their dangling bonds so that they are motionless and are regarded as bulk atoms. The observed bulk lattice constant of Si, 5.43072 Å [15], is used to set up the two-dimensional lattice. Chadi [16] has shown that for the Si(100) surface atomic relaxations extend over the first five layers. Since the atomic displacement for the fifth-layer atom was calculated to be only 0.034 Å [16], we believe the use of a fixed fifth layer may be adequate for studying relative preference between perpendicular and parallel line defects. (Here, "perpendicular" and "parallel" are defined with respect to the dimer rows.) The line defect is modeled by a *periodic array* of infinitely long missing atomic lines. Figures 4(a) and 4(b) correspond to line defects which are perpendicular and parallel to the dimer rows, respectively. Because of the usual computer constraints, we could realistically only consider the lower limit of the line-defect width. In the perpendicular case (i), the line defect is a single missing atomic line repeating itself periodically every fourth line. The unit cell contains 38 atoms, i.e., 6 in the surface layer and 8 per layer in the second to fifth layers. As shown in Fig. 4(a), exposed second-layer atoms have the freedom to form dimers; whether they form dimers is to be determined by the MD simulations, which allow all atoms except those in the bottom layer to settle to their most stable positions.

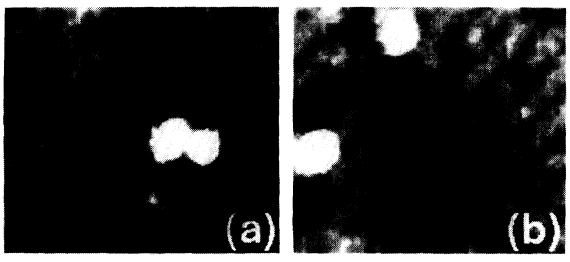

FIG. 3. STM images of two large craters caused by a 3-keV Ar^+-ion bombardment. Area is 6 nm×6 nm.

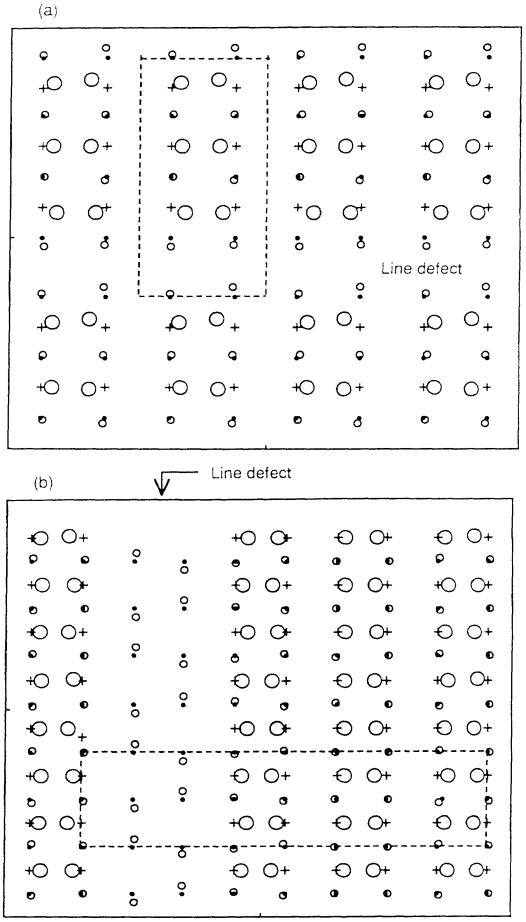

FIG. 4. Molecular-dynamics simulations of a periodic array of line defects on the Si(100)-(2×1) surface. (a) Line defects perpendicular to dimer rows, case (i); and (b) line defect parallel to dimer rows, case (ii). The small crosses and the solid dots are ideal unrelaxed positions for surface- and second-layer atoms, respectively. The rectangle enclosed by dashed lines is the unit cell.

For the parallel case shown in Fig. 4(b), denoted as case (ii), the periodic line defects are in the form of a single missing dimer row (i.e., twin missing atomic lines) repeating every fourth dimer row. The choice of twin missing atomic lines is to keep the ratio between the number of missing atoms and surface atoms in a unit cell the same as that for case (i) so that the comparison of total energies is meaningful. We choose a unit cell twice as large as that of case (i). There are 76 atoms per unit cell, 12 in the surface layer and 16 per layer in the second to fifth layers. This choice of a doubled unit cell is to allow the exposed second-layer atoms freedom to form dimers. For both cases (i) and (ii) we use the single two-dimensional special point of Cunningham [17] for a rectangular lattice and its reflectionally symmetric points with respect to x and y axes and the inversion symmetric point to optimize atomic positions. To compare total energies (per atom) between cases (i) and (ii), we find that the use of 16 two-dimensional special points of Cunningham [17] is quite adequate. We have also tested the use of 64 special points and it essentially yields the same results.

Figures 4(a) and 4(b) show the lateral displacements of surface- and second-layer atoms from their ideal unrelaxed atomic positions. In both cases (i) and (ii) dimerization directions of surface atoms and exposed second-layer atoms can be seen perpendicular to each other as stated previously. Surface atoms form buckled (not shown in Fig. 4) asymmetric dimers similar to those discussed by Chadi [16]. In case (i), the second-layer dimerization is not very pronounced and the atomic pairs have bond lengths (2.86 Å) much larger than that of surface dimers (2.36 Å). This is because each exposed second-layer atom is still bonded to and drawn towards a surface atom at either edge of the line defect. We have performed charge-density calculations and find that the charge density is significantly large in the central region of each atom pair in the exposed layer to indicate that the atom pairs indeed form dimers through their single dangling bonds. It is interesting to note that in case (ii), the two second-layer dimer lines in the defect are not in phase. They are approximately out of phase by about 180°. This arrangement exerts less strain on third-layer atoms bridged between these two second-layer dimer lines than when they are in phase.

We find that the total energy for case (i) is about 0.011 eV/atom lower than that for case (ii), favoring line defects perpendicular to dimer rows as shown in the STM images Figs. 1(c) and 1(d). The lower total energy for case (i) may be qualitatively understood from the shorter bonding distance (and hence stronger bonding) between an exposed second-layer atom and a surface atom at either edge of the line defect as shown in Fig. 4(a). However, the preference for case (i) is partly compensated by the restriction of exposed-second-layer dimerization, as stated earlier, and by the interruption of the (2×1) dimer rows. In contrast, the exposed second-layer atoms in case (ii) have less constraint to form dimers and have no interruption of dimer rows as shown in Fig. 4(b). This may be the reason that the calculated total energy difference is small.

In a recent report by Bedrossian and Klitsner [18], Si(100)-(2×1) surfaces were bombarded by 225-eV Xe^+ ions at grazing incidence along the [110] direction at temperatures 400–450 °C. They observed retraction of S_B step edges as well as monolayer-deep depressions or "vacancy islands" elongated parallel to the dimer rows. However, in contrast to the present report, the structures they observed are not equilibrium structures, but are structures stabilized at moderately high temperatures, i.e., ~450 °C, by kinetic considerations, analogous with growth.

In summary, we have obtained good agreement between molecular-dynamics simulations and STM images of random and ordered defects produced by energetic ion impacts on the Si(100)-(2×1) surface.

We thank Peter Bedrossian for his useful comments and suggestions on the manuscript. I.S.T.T. thanks Philips Research Laboratories for the award of a van Houten Fellowship. M.-H.T. and J.D.D. acknowledge support from U.S. Army Research Office (DAAL03-91-G-0054).

[1] H. J. W. Zandvliet, H. B. Elswijk, E. J. van Loenen, and I. S. T. Tsong, Phys. Rev. B **46**, 7581 (1992).
[2] H. Niehus, U. K. Koehler, M. Copel, and J. E. Demuth, J. Microsc. **152**, 735 (1988).
[3] A. H. M. Holtslag and A. van Silfhout, Surf. Sci. **187**, 36 (1987).
[4] A. H. M. Holtslag, U. C. Slager, and A. van Silfhout, Surf. Sci. **152/153**, 1079 (1985).
[5] H. J. C. Berendsen, J. P. M. Postma, W. F. van Gunsteren, A. DiNola, and J. R. Haak, J. Chem. Phys. **81**, 3684 (1984).
[6] F. H. Stillinger and T. A. Weber, Phys. Rev. B **31**, 5262 (1985).
[7] I. M. Torrens, *Interatomic Potentials* (Academic, New York, 1972).
[8] R. Smith, D. E. Harrison, and B. J. Garrison, Phys. Rev. B **40**, 3979 (1989).
[9] P. C. Zalm, J. Appl. Phys. **54**, 2660 (1983).
[10] H. Kahata and K. Yagi, Jpn. J. Appl. Phys. **28**, L1042 (1989).
[11] O. F. Sankey and D. J. Niklewski, Phys. Rev. B **40**, 3979 (1989).
[12] O. F. Sankey, D. J. Niklewski, D. A. Drabold, and J. D. Dow, Phys. Rev. B **41**, 12750 (1990).
[13] G. B. Adams and O. F. Sankey, Phys. Rev. Lett. **67**, 867 (1991).
[14] G. B. Adams, J. B. Page, O. F. Sankey, K. Sinha, and J. Menendez, Phys. Rev. B **44**, 4052 (1991).
[15] *CRC Handbook of Chemistry and Physics*, edited by D. R. Lide (CRC Press, Boca Raton, 1991–1992), 72nd ed.
[16] D. J. Chadi, Phys. Rev. Lett. **43**, 43 (1979).
[17] S. L. Cunningham, Phys. Rev. B **10**, 4988 (1974).
[18] P. Bedrossian and T. Klitsner, Phys. Rev. Lett. **68**, 646 (1992).

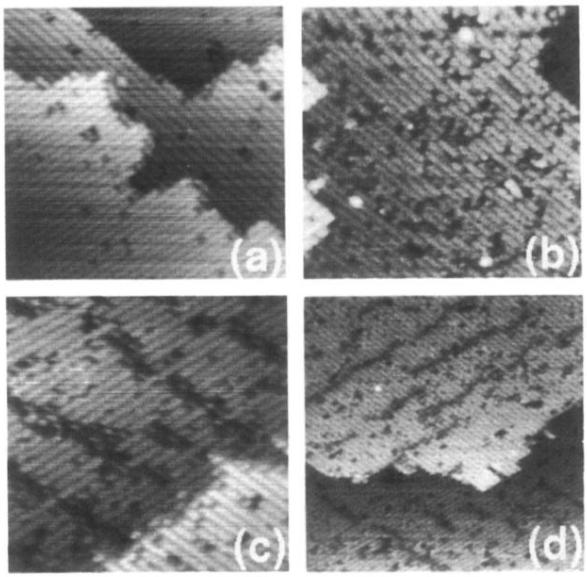

FIG. 1. Filled-state STM images of Si(100)-(2×1) surfaces taken at sample bias of −2 V and tunnel current 0.5 nA. (a) Clean surface prior to bombardment. Scan area is 28 nm×28 nm. (b) After bombardment by 3-keV Ar^+ ions at a dose of 1.5×10^{12} ionscm^{-2}. Scan area is 26 nm×26 nm. (c) Bombarded surface after annealing at 600 °C for 2 min. Scan area is 22 nm×22 nm. (d) Bombarded surface after annealing at 750 °C for 2 min. Scan area is 40 nm×40 nm.

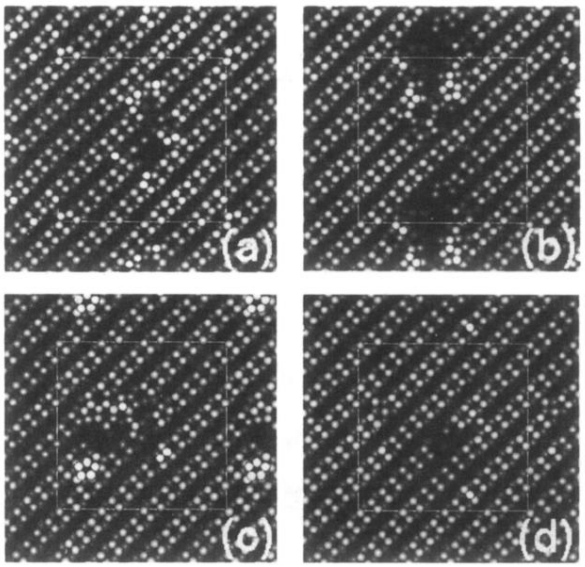

FIG. 2. Ion-impact craters produced by molecular-dynamics simulations. (a) A double crater. (b) A large crater. (c) A medium crater. (d) A small crater. The craters in (b) and (c) appear double because of periodic boundary conditions.

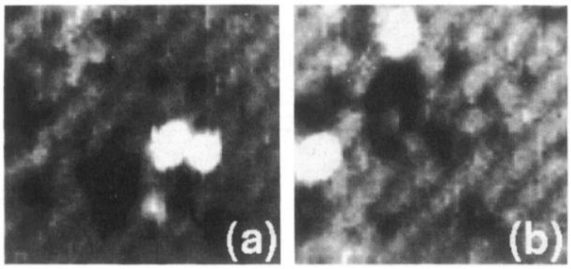

FIG. 3. STM images of two large craters caused by a 3-keV Ar^+-ion bombardment. Area is 6 nm×6 nm.